Prediction of Microstructure in Laser Deposition of Titanium Alloys

N.W. Klingbeil, C.J. Brown, S. Bontha
Department of Mechanical and Materials Engineering
Wright State University
Dayton, OH, 45435

P.A. Kobryn
Materials and Manufacturing Directorate (AFRL/MLLMP)
Air Force Research Laboratory
WPAFB, OH 45433

H.L. Fraser
Department of Materials Science and Engineering
The Ohio State University
Columbus, OH 43210

Abstract

Laser deposition of titanium alloys is under consideration for aerospace applications, and offers significant increases in efficiency and flexibility compared to conventional manufacturing methods. However, its ultimate success will depend on the ability to predict and control the microstructure and resulting mechanical properties of the deposit. In this study, both 2-D continuum finite element modeling and 3-D cellular automaton finite element modeling of a thin-wall geometry are used to investigate the effects of deposition process variables on microstructure in laser deposited Ti-6Al-4V. Numerical results for cooling rate and thermal gradient obtained from the 2-D models are used to provide insight into grain size and morphology, while the 3-D cellular automaton models are used to provide direct predictions of deposited microstructure. The numerical model predictions are subsequently compared with observed microstructures in LENS™ deposited Ti-6Al-4V.

Introduction

Laser deposition of titanium alloys is currently being considered for aerospace applications, because it can substantially reduce both the buy-to-fly ratio and production lead time compared with conventional manufacturing methods [1-2]. Moreover, laser-based material deposition will potentially enable the direct manufacture of advanced aerospace components made of multiple or functionally graded materials [3], or smart structures containing embedded sensors or electronic components. Finally, the flexibility of laser deposition allows virtually unlimited creation of advanced alloys through the use of elemental blends [4], which may ultimately spawn the next generation of aerospace materials.

Despite their strong potential, the success of laser-based SFF processes as viable manufacturing alternatives for aerospace components may ultimately hinge on the ability to consistently control microstructure and resulting mechanical properties. To date, only limited experimental data exist to link laser deposition process variables to resulting microstructure and mechanical properties in titanium alloys [5-7], and suitable microstructures have typically been obtained only through trial and error. Thus, simulation-based methods are needed to predict the effects of process variables (e.g., laser power and velocity) on microstructure in laser deposited titanium and other aerospace materials.

In this study, both 2-D continuum finite element modeling and 3-D cellular automaton modeling of a thin wall geometry are used to investigate the effects of laser power and velocity on microstructure (grain size and morphology) in laser-deposited Ti-6Al-4V. Continuum finite element modeling of laser deposition processes is fairly well established, and has been successfully used to study the effects of process variables on melt-pool size and residual stress [8-11]. Cellular automaton modeling has been applied to laser deposition of aluminum alloys [12], and shows strong potential for linking process variables with microstructure in laser-based material deposition. In the upcoming sections, cooling rates and thermal gradients extracted from the 2-D models are used to provide insight into the effects of laser power and velocity on grain size and morphology, while the 3-D models are used to provide direct predictions of microstructure in laser-deposited Ti-6Al-4V. The numerical model predictions are subsequently compared with observed microstructures obtained using the LENS™ process.

Thin Wall Geometry Considered

The scope of the current study has been limited to a particular thin wall geometry, as shown in Figure 1. The chosen geometry is representative of thin-wall structures commonly built using the LENS™ process, and has been used to investigate the effects of laser power Q and velocity V over the range of Ti-6Al-4V process variables tabulated below.

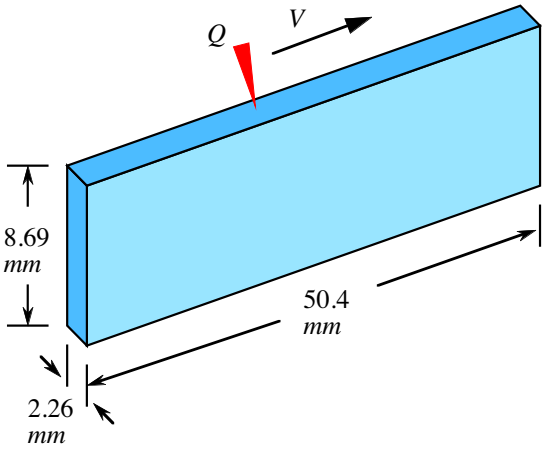

Laser Power, Q (W)	Laser Velocity, V (mm/s)		
315	6.35	8.47	10.6
350	6.35	8.47	10.6
385	6.35	8.47	10.6

Figure 1. Thin Wall Geometry and Range of Process Variables Considered

Test specimens of the above geometry have been manufactured using the Optomec LENS™ 750 system at Ohio State University over the full range of tabulated process variables. In the upcoming sections, numerical modeling of the same geometry is used to predict the effects on microstructure (grain size and morphology) of changes in laser power and velocity, and results are subsequently compared to observed microstructures in the deposited specimens.

2-D Thermal Finite Element Modeling

The goal of the 2-D thermal finite element modeling adopted herein is to determine the effects of laser power and velocity on cooling rate and thermal gradient, which are the primary parameters responsible for grain size and morphology in Ti-6Al-4V. While the cooling rate is largely responsible for grain size, it is the combination of cooling rate and thermal gradient at the onset of solidification which is responsible for grain morphology (generally classified as either equiaxed, columnar or mixed) [1-2]. In this section, cooling rates and thermal gradients are extracted from 2-D model results for the geometry of Fig. 1, and are used to provide insight into the effects of laser power and velocity on both grain size and morphology.

Numerical Modeling Procedures

The 2-D thermal finite element modeling procedures adopted herein are analogous to those used by Vasinonta *et al.* [8-10] in studies of melt-pool size and residual stress in laser deposition of thin-wall stainless steel structures. A representative 2-D finite element mesh of the thin wall geometry of Fig. 1 is illustrated in Fig. 2a. The model uses 4-noded bi-linear thermal elements, and has been generated using the software package ABAQUS.

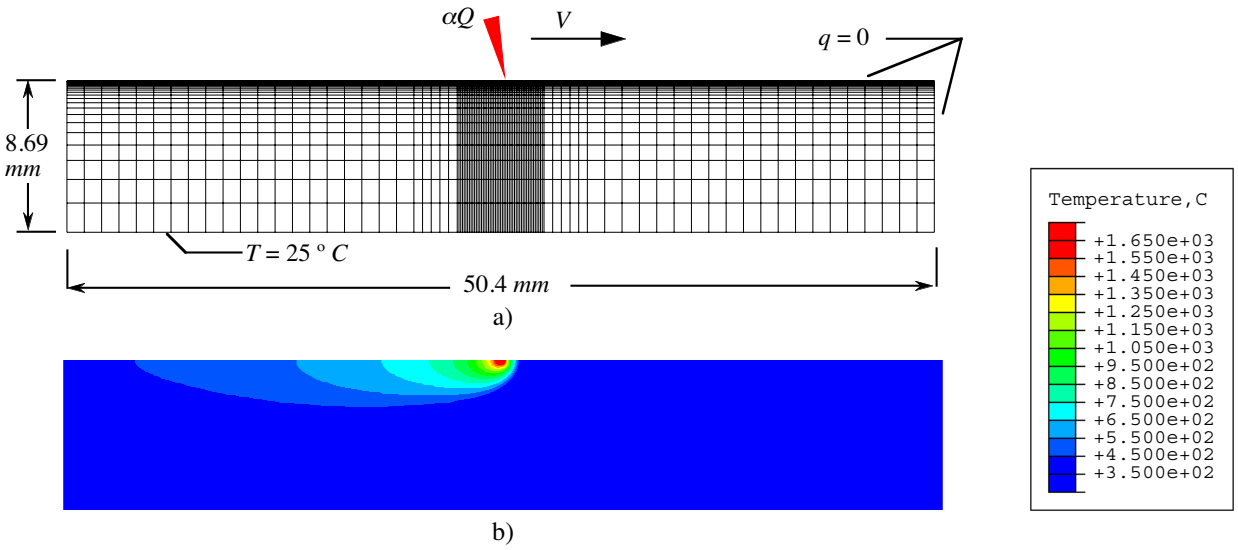

Figure 2. a) Representative 2-D Thermal Finite Element Mesh and b) Temperature Contours for $Q = 350$ *W* and $V = 8.47$ *mm/s*

The finite element model approximates the laser deposition process as a moving point heat source αQ, which is successively applied to adjacent nodes (beginning at the left end) at time intervals corresponding to the laser velocity V. The parameter α represents the fraction of the laser power absorbed by the deposit, and based on previous results in the literature has been estimated as 35% [10]. The remaining boundary conditions are approximated as insulated ($q = 0$) on the top and both vertical edges, with a fixed temperature condition on the bottom ($T = 25\ ^{o}C$). As discussed by Vasinonta *et al.* [8-10], the presence of natural convection on the edges is essentially equivalent to thermal insulation. While the fixed room temperature condition on the bottom neglects any inherent preheating of the base during material deposition, its effect on thermal gradient and cooling rate in close proximity to the laser (i.e., within the melt pool) is assumed to be small. Finally, the finite element model uses temperature-dependent specific heat, density and thermal conductivity, and includes latent heat effects for Ti-6Al-4V.

A representative contour plot illustrating the transient temperature distribution is illustrated in Fig. 2b for the case of $Q = 350$ *W* and $V = 8.47$ *mm/s*. The location of the laser is evident from the intensity of the temperature distribution, where the maximum contour limit of 1650 ^{o}C signifies the melt pool. As shown in the figure, the thermal history is essentially independent of the vertical free-edges once the laser has reached the center of the wall, where the mesh has been highly refined for accurate extraction of the thermal gradient and cooling rate. In general, the mesh resolution of Fig. 2 has provided more than 10 elements through the depth of the melt pool (roughly 200 μm), so that both thermal gradient and cooling rate at the onset of solidification can be determined as a function of vertical location beneath the surface.

Extraction of Cooling Rate and Thermal Gradient

The cooling rate and thermal gradient at the onset of solidification have been extracted from the 2-D model results at various nodal locations throughout the depth of the melt pool. At each nodal location, the solidification cooling rate is determined as

$$\frac{\partial T}{\partial t} = \left| \frac{T_s - T_L}{t_s - t_L} \right|, \tag{1}$$

in which T_L and T_s are the liquidus and solidus temperatures reached at times t_L and t_s, respectively. As defined in eq. (1), the cooling rate is an average value taken throughout the time required for solidification, which is typically on the order of 10^{-3} seconds. The thermal gradient evaluated at the time $t = t_L$ is determined directly from the nodal heat flux output, and is obtained from Fourier's Law as

$$G = \left| \vec{\nabla} T \right| = \frac{|\vec{q}|}{k}, \tag{2}$$

in which $|\vec{q}|$ is the magnitude of the heat flux vector and k is the thermal conductivity at the liquidus temperature, T_L. Finally, the solidification cooling rate and thermal gradient determine the solidification velocity R as

$$R = \frac{1}{G}\frac{\partial T}{dt}. \tag{3}$$

Following the calculation of G and R, the expected grain morphology can be predicted as either equiaxed, columnar or mixed by plotting points in G vs. R space (i.e., on the "solidification map") [1-2]. In the upcoming section, results for thermal gradient and cooling rate are interpreted in the context of the solidification map to predict the effects of laser power and velocity on grain morphology.

2-D Model Results

Numerical results illustrating the effects of laser power and velocity on cooling rate, thermal gradient and predicted grain morphology are summarized in Figs. 3-4. The effect of laser power for a fixed laser velocity of $V = 8.47$ *mm/s* is illustrated in Figs 3a-3b, in which cooling rate and thermal gradient at the onset of solidification are plotted as a function of depth within the melt pool. The substantial spatial variance of both cooling rate and thermal gradient are indicative of the complexities associated with temperature-dependent material properties and nonlinear latent heat effects. Still, the results of Fig. 3a clearly indicate that for a fixed laser velocity, an increase in laser power causes a decrease in solidification cooling rate throughout the depth of the melt pool. This would suggest an increase in grain size with laser power, which is in keeping with experimental results in the literature [5].

The results of Fig. 3b indicate a similar relationship for thermal gradient, which also decreases with increasing laser power. This result is in keeping with thermal gradient process maps previously reported in the literature [9], although the latter were evaluated at temperatures well below the melting point for use in residual stress prediction. In order to provide insight into grain morphology, the data plotted in Figs. 3a-3b were related through eq. (3), and are plotted on the solidification map of Fig. 3c. The solid and dashed lines of Fig. 3c bound the regions of fully equiaxed, fully columnar and mixed grain morphologies, as previously calibrated for Ti-6Al-4V [1-2]. Despite the spatial variances in Figs. 3a and 3b, the data points for all powers and depths are

clustered in the fully columnar region of Fig. 3c. This result is in keeping with previous results obtained for laser passes across plate-shaped (as opposed to thin-wall) substrates [1-2].

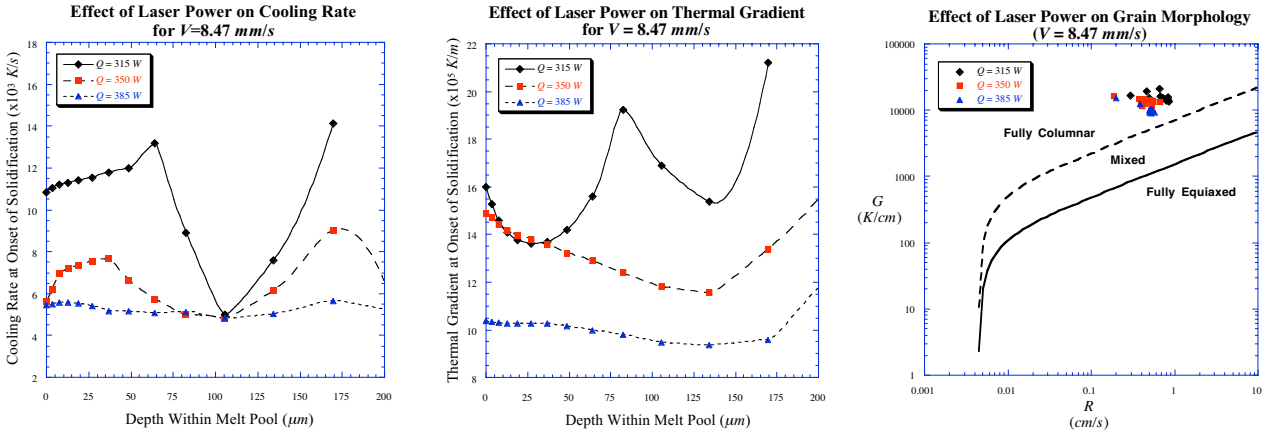

Figure 3. Effect of Laser Power on a) Cooling Rate, b) Thermal Gradient and c) Predicted Grain Morphology for $V = 8.47$ *mm/s*

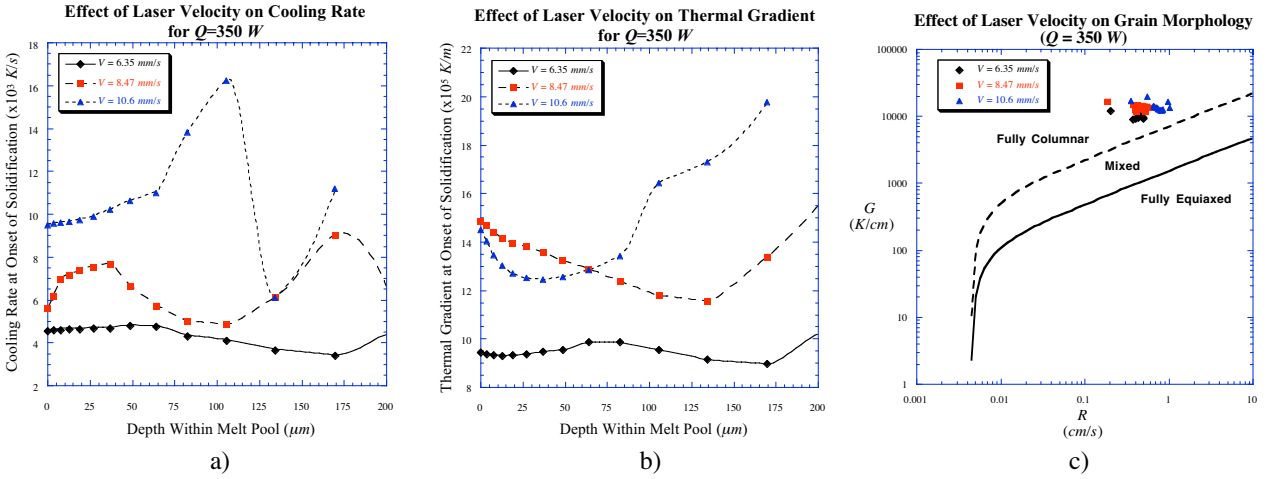

Figure 4. Effect of Laser Velocity on a) Cooling Rate, b) Thermal Gradient and c) Predicted Grain Morphology for $Q = 350$ *W*

The effects of laser velocity on solidification cooling rate, thermal gradient and predicted grain morphology are shown in Fig. 4 for the case of $Q = 350$ *W*. The results of Fig. 4a show that cooling rate increases with laser velocity, which would indicate a decrease in grain size. When considered together, the cooling rate results of Figs. 3a and 4a suggest that grain size increases with incident energy (the ratio of laser power to velocity), which is in keeping with experimental results previously reported in the literature [5]. On the other hand, trends in thermal gradient with laser velocity are less straightforward, and according to Fig. 4b depend on depth within the melt pool. In particular, the results suggest that thermal gradient increases monotonically with laser velocity only beyond a depth of roughly 65 *μm*. That said, when the results of Figs. 4a and 4b are related through eq. (3), the predicted grain morphologies illustrated in Fig. 4c are essentially still clustered in the fully columnar range.

3-D FEM and Cellular Automaton Modeling

The goal of the 3-D modeling discussed here is to provide direct predictions of grain size and morphology as a function of laser power and velocity for the thin-wall geometry of Fig. 1. Although the thermal problem for the geometry of Fig. 1 is essentially two dimensional, the grain nucleation and growth process is inherently three dimensional, and requires nodal temperature input from a 3-D analysis. The general procedures used here involve 3-D thermal finite element modeling of the laser deposition process using the software package ProCast™, followed by 3-D cellular automaton solidification modeling of grain nucleation and growth using the software package CAFE3D.

Detailed background on the cellular automaton algorithms used in CAFE3D can be found in [13]. In brief, the software uses a Gaussian distribution of nucleation sites to simulate the stochastic nucleation process, and a deterministic third-order equation to describe grain growth during solidification. It requires statistical nucleation parameters for the material system of interest (specifically nucleation site density, mean nucleation undercooling, and standard deviation of the undercooling), which, in the case of Ti-6Al-4V, have been calibrated by direct comparison with cast ingots of varying size [14]. A description of the 3-D modeling and procedures used to link the ProCast™ and CAFE3D analyses is provided below, followed by a comparison of model predictions and observed microstructures in LENS™ deposited specimens.

Numerical Modeling Procedures

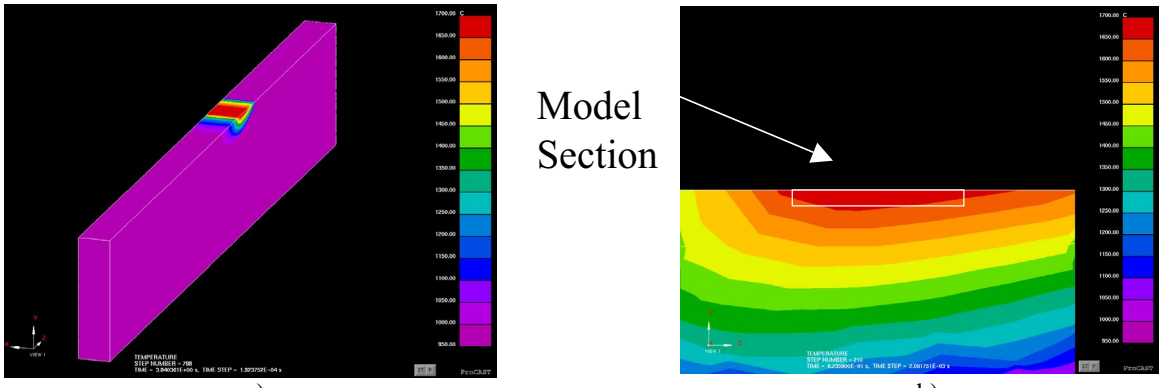

a) b)

Figure 5. a) ProCast™ Temperature Contours for Q = 350 W and V = 8.47 mm/s and b) Section of Model Used in CAFE3D Cellular Automaton Analysis

The 3-D thermal finite element procedures (ProCast™) were similar to those used in the 2-D models, with identical input properties for Ti-6Al-4V. The primary difference in the modeling was the application of the applied heat flux boundary condition (i.e., the moving laser), which was modeled as a uniformly distributed heat source successively applied over 50 equally-spaced regions along the top surface. As seen in Fig. 5a, the resulting temperature contours for the case of Q = 350 W and V = 8.47 mm/s were similar to those obtained for the 2-D models (Fig. 2b), in which the laser was modeled as a point heat source. While the uniform heat flux in the 3-D model results in a somewhat broader region of temperatures above 1000 ^oC, the depth of the melt pool was comparable to that obtained in the 2-D model.

For a given set of process variables (i.e., laser power and velocity), thermal history output from the ProCast™ model was used as input for subsequent CAFE3D cellular automaton analysis of grain nucleation and growth. However, because the CAFE3D software is designed to start from an

entirely liquid state, it was necessary to first isolate the melt pool region from the ProCast™ model. As illustrated in Fig. 5b, thermal history data from the section of the model within the melt pool (i.e., $T > 1650\ ^{o}C$) were extracted from the ProCast™ model and used to define an equivalent melt-pool model suitable for CAFE3D analysis. Because the temperature data within the melt pool are representative of a given combination of laser power and velocity, this enabled direct prediction of grain size and morphology as a function of process variables.

CAFE3D Predictions and Comparison with Observed Microstructures

A sample comparison of predicted and observed LENS™ microstructures is shown in Fig. 6 for the case of $Q = 350\ W$ and $V = 10.6\ mm/s$. Also tabulated in the figure is a comparison of predicted and observed grain sizes over the full range of process variables considered.

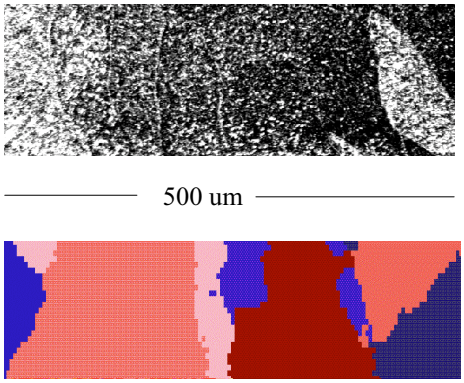

Laser Power (W) ($V = 8.47\ mm/s$)	Grain Size (μm)	
	CAFE3D	Observed
315	125	104
350	91	83
385	83	58

Laser Velocity (mm/s) ($Q = 350\ W$)	Grain Size (μm)	
	CAFE3D	Observed
6.35	77	71
8.47	91	83
10.6	83	77

Figure 6. Comparison of CAFE3D Predictions and Observed Microstructures

In general, reasonable agreement was obtained between CAFE3D-predicted and observed grain morphologies, which were fully columnar over the full range of process variables considered. This result was expected based on both the 2-D model predictions and previous results in the literature [5]. Good agreement was also obtained between CAFE3D predictions and observed grain sizes; however, trends in both the predicted and observed grain sizes were in contrast to both the 2-D model predictions and previously published results [5]. Namely, both the predicted and observed grain sizes actually *decreased* with increasing laser power, and neither showed a monotonic decrease in grain size with increasing laser velocity. A possible explanation for these anomalous trends in grain size is the relatively few number of grains within the melt pool (see Fig. 6), which may be insufficient to warrant a statistically meaningful result. This issue remains a topic of ongoing research.

Conclusions

In this study, both 2-D continuum finite element modeling and 3-D cellular automaton modeling were used to investigate the effects of laser power and velocity on grain size and morphology in thin-wall Ti-6Al-4V deposits. Both the 2-D and 3-D models predicted fully columnar microstructures, which was in keeping with experimental observations. While trends in cooling rate and thermal gradient obtained from the 2-D models suggested an increase in grain size with increasing power/velocity ratio, this result was supported by neither the 3-D model predictions nor the observed LENS™ microstructures. A contributing factor is suspected to be the relatively large size of the grains compared to the melt pool, which leads to increased variability in both actual microstructures and CAFE3D predictions. Still, the 2-D thermal finite element modeling and 3-D cellular automaton modeling presented here have shown the potential to be valuable tools for predicting microstructure in laser deposited materials.

Acknowledgments

This work was supported by the Joint AFRL/DAGSI Research Program, project number ML-WSU-01-11, as well as by a grant from Wright State University and the Ohio Board of Regents. The authors would also like to thank David Bryan and Matthew Slaughter of Ohio State University for preparing the LENS™ specimens used in this work.

References

1. Kobryn, P.A. and Semiatin, S.L., 2000, "Laser Forming of Ti-6Al-4V: Research Overview," *Solid Freeform Fabrication Proceedings*, (D.L. Bourell, J.J. Beaman, R.H. Crawford, H.L. Marcus and J.W. Barlow, eds.), Austin, August 2000.

2. Kobryn, P.A. and Semiatin, S.L., 2001, "The Laser Additive Manufacture of Ti-6Al-4V," *JOM*, September 2001.

3. Jackson, T.R., Liu, H., Patrikalakis, N.M., Sachs, E.M., and Cima, M.J., 1999, "Modeling and Designing Functionally Graded Material Components for Fabrication with Local Composition Control," *Journal of Materials and Design*, Vol. 20, No. 2/3, pp. 63-75.

4. Schwendner, K.I., Banerjee, R., Collins, P.C. , Brice, C.A. and Fraser, H.L., 2001, "Direct Laser Deposition of Alloys from Elemental Powder Blends," *Scripta Materiala*, Vol. 45, pp. 1123-1129.

5. Kobryn, P.A., Moore, E.H. and Semiatin, S.L., 2000, "The Effect of Laser Power and Traverse Speed on Microstructure, Porosity and Build Height in Laser-Deposited Ti-6Al-4V," *Scripta Materiala,* Vol. 43, pp. 299-305.

6. Kobryn, P.A. and Semiatin, S.L., 2001, "Mechanical Properties of Laser-Deposited Ti-6Al-4V," *Solid Freeform Fabrication Proceedings*, (D.L. Bourell, J.J. Beaman, R.H. Crawford, H.L. Marcus and J.W. Barlow, eds.), Austin, August 2001.

7. C. A. Brice, K. I. Schwendner, D. W. Mahaffey, E. H. Moore, and H. L. Fraser, 1999, "Process Variable Effects On Laser Deposited Ti-6Al-4V, *Solid Freeform Fabrication Proceedings*, (D.L. Bourell, J.J. Beaman, R.H. Crawford, H.L. Marcus and J.W. Barlow, eds.), Austin, August 1999.

8. Vasinonta, A., Beuth, J.L. and Griffith, M.L.,1999, "Process Maps for Laser Deposition of Thin-Walled Structures," *Solid Freeform Fabrication Proceedings*, (D.L. Bourell, J.J. Beaman, R.H. Crawford, H.L. Marcus and J.W. Barlow, eds.), Austin, August 1999, pp. 383-391.

9. Vasinonta, A., Beuth, J.L. and Griffith, M.L., 2000, "Process Maps for Controlling Residual Stress and Melt Pool Size in Laser-Based SFF Processes," *Solid Freeform Fabrication Proceedings*, (D.L. Bourell, J.J. Beaman, R.H. Crawford, H.L. Marcus and J.W. Barlow, eds.), Austin, August 2000, pp. 200-208.

10. Vasinonta, A., Beuth, J.L. and Griffith, M.L., 2001, "A Process Map for Consistent Build Conditions in the Solid Freeform Fabrication of Thin-Walled Structures," *Journal of Manufacturing Science and Engineering*, Vol. 123, No. 4, pp. 615-622.

11. Beuth, J.L. and Klingbeil, N.W., 2001, "The Role of Process Variables in Laser-Based Direct Metal Solid Freeform Fabrication," *JOM*, Vol. 53, No. 9, pp. 36-39.

12. Grujicic, M. Cao, G. and Figliola, R.S., 2001, "Computer Simulations of the Evolution of Solidification Microstructure in the LENS™ Rapid Fabrication Process," *Applied Surface Science*, Vol. 183, pp. 43-47.

13. Gandin, Ch. A., Desbiolles, J.L., Rappaz, M. and Thevoz, Ph., 1999, "A Three-Dimensional Cellular Automaton-Finite Element Model for the Prediction of Solidification Grain Structures," *Metallurgical and Materials Transactions A*, Vol. 30A, pp. 3153-3165.

14. Brown, C.J., Klingbeil, N.W. and Kobryn, P.A., "Prediction of Microstructure in Laser Deposition of Ti-6Al-4V," *AIAA Dayton-Cincinnati Aerospace Science Symposium,* Dayton, OH, April 2002.